Pure Appl. Geophys. 176 (2019), 279–295

https://doi.org/10.1007/s00024-018-2023-6

Pure and Applied Geophysics

The 1963 Vajont Landslide: A Numerical Investigation on the Sliding Surface Heterogeneity

Filippo Zaniboni[1] and Stefano Tinti[1]

Abstract—The 1963 Vajont landslide is a key case in landslide literature, because it was catastrophic and because a lot of accurate data were collected before and after its occurrence. In this paper, the main focus is on the possible heterogeneity of the sliding surface involved by the landslide motion, which is reflected by a heterogeneous distribution of the dynamic basal friction coefficient μ. Assuming a given zonation of the sliding surface, our strategy was to apply a 2D Lagrangian model to compute the landslide motion and to find the values of μ for each zone, leading to the best agreement between the computed and the observed final deposit. Following some hints from the literature, we have explored heterogeneous configurations composed of up to four different zones, including also the homogeneous case, by means of a 2D numerical model (UBO-BLOCK2) that handles the landslide as a mesh of blocks and runs quickly enough to allow the computation of tens of thousands of simulations in a reasonable computing time. It is found that the four-zone zonation produces the best fit (or the least misfit), which is a strong hint that the gliding surface involved different geotechnical units.

Key words: Vajont landslide, Lagrangian approach, numerical simulations, friction coefficient, misfit.

1. Introduction

The 1963 Vajont landslide, before and after its occurrence, raised a lot of discussions and inspired several studies in the scientific community. Of this event, only the essential features are reported here since, for a detailed account, one can refer to previous works such as the ones by Hendron and Patton (1985), by Semenza and Ghirotti (2000) and by Genevois et al. (2005).

On October 9, 1963, a huge mass with an estimated volume of about 260 million m^3, collapsed into the Vajont reservoir (that was created some years earlier by building a 260-m-high dam) following a series of basin-emptying and basin-filling events. The landslide, moving northwards from the northern flank of Mt. Toc (see Fig. 1 for toponyms), crashed into the basin. It displaced 40 million m^3 of water that ran up the opposite side of the valley, almost reaching the village of Casso, more than 200 m above the reservoir level. Part of the water either travelled upstream towards the village of Erto or splashed back over the slide mass, forming a temporary lake. Most of the water (25 million m^3, Selli and Trevisan 1964) unfortunately channeled westward down the Vajont gorge (Fig. 1) and reached the Piave valley, where it caused a disaster. The water, mud and debris flow left more than 2000 casualties and destroyed 5 villages, the most populated of which was Longarone.

This tragedy had a wide resonance in the media due to the large death toll, but also for issues concerning the management of the reservoir: the slide, in fact, was already known, studied and monitored since at least 3 years before the catastrophic event (Semenza and Ghirotti 2000).

For the scope of our paper, it is convenient to briefly summarize the state of the art as regards the shape and nature of the sliding surface and the estimates of the friction coefficient. After the failure, an extensive area remained uncovered on the steep slope uphill, still visible today (Fig. 1, between the red and the green lines): this is mainly, but not entirely, composed of clay, resulting from the exposure of different alternating thin clay layers. This feature induced Carloni and Mazzanti (1964) to hypothesize the existence of a well-defined sliding surface connecting the 45°-dip clay layers on the top to the nearly horizontal layers visible at the bottom. Selli and Trevisan (1964) assumed that the sliding zone was located mainly within the clay layers and that the sliding surface had a "chair-like" shape on the

[1] Dipartimento di Fisica e Astronomia, Alma Mater Studiorum-Università di Bologna, Bologna, Italy. E-mail: filippo.zaniboni@unibo.it

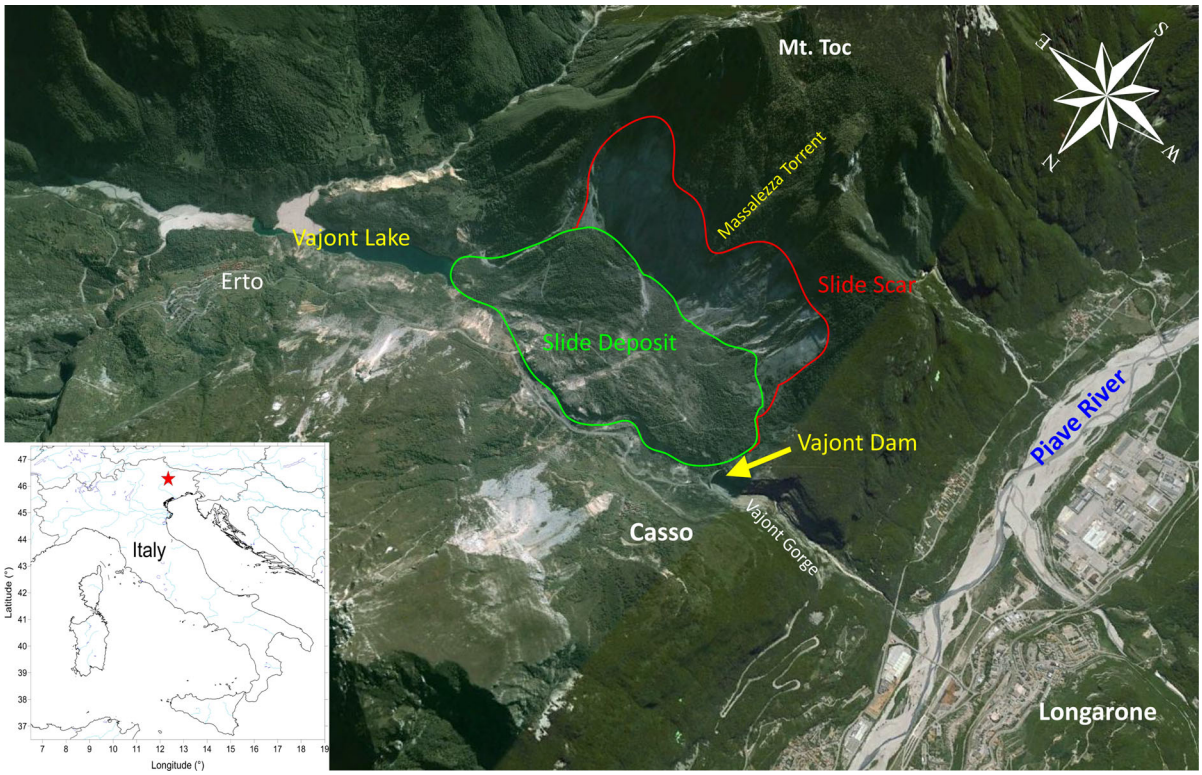

Figure 1
Map of the Vajont valley (NE Italy), viewed from the NW, modified after Google Earth©, with indications of the main toponyms. The red line marks the upper portion of the sliding surface; the green line is the boundary of the 1963 deposit

westside and a parabolic shape in the eastside. This idea was widely accepted after Hendron and Patton's report (1985), who also confirmed the view that the slide was a reactivation of a prehistoric event (see also Paronuzzi and Bolla 2012). However, worthy of notice is that a very recent work by Dykes and Bromhead (2018a), recalling and expanding results by Bistacchi et al. (2013) and by Petronio et al. (2016), has reopened the discussion putting some doubts on the previous conclusions. In particular, they claim that the "chair-like" shape of the western part of the sliding surface has to be reconsidered, together with the hypothesis of an old landslide reactivation.

As for the landslide dynamics, Ciabatti (1964) evaluated a maximum velocity of 17 m/s, an initial acceleration of about 0.1 m/s^2, a 450-m run-out, and a motion duration of 45 s. This last feature was supported by seismic records analyses (Caloi 1966). The most interesting result by Ciabatti (1964) is the value he obtained for the friction coefficient, i.e. μ = 0.236 (corresponding to a friction angle ϕ of 13°). Hendron and Patton (1985) found even lower values for the friction angle (actually 6°–10°) in laboratory tests on clay-rich layers. But the most suitable value in the field for them for ϕ was about 12° to account for irregularities in the slip surface and rock-to-rock contact. Further studies supported very low values, invoking several mechanisms reducing the basal resistance, and are mentioned here only for the sake of completeness: (1) loss of strength when the material is affected by high shear rate (Semenza and Ghirotti 2000; Tika and Hutchinson 1999); (2) sudden fracturing of the sliding mass, causing drop of resisting stress (Kilburn and Petley 2003); (3) pore pressure increased by seismicity (Mantovani and Vita-Finzi 2003); (4) thermic effects decreasing the shearing resistance (Cecinato et al. 2011; Pinyol and Alonso 2010; Vardoulakis 2002); and (5) formation

of a water film, not necessarily vaporized, abruptly reducing the friction to zero (Ferri et al. 2011).

The 1963 Vajont event has been studied by several authors by means of numerical models. Sitar et al. (2005), using a block model and assuming a unique friction angle $\phi = 12°$, obtained a velocity peak of 20 m/s. More recently, Crosta et al. (2016) and Zhao et al. (2016) modelled the slide and the consequent water flow using a 3D finite element method (FEM) code and a coupled discrete element method-computational fluid dynamics (DEM-CFD) code, respectively. In both studies, homogeneous low friction values were obtained, namely $\phi = 6°$ in the first and $\phi = 10°$ in the second, leading to peak speed values around 25 m/s.

Very interesting is that several studies (e.g. Superchi 2012; Bistacchi et al. 2013; Wolter et al. 2014, 2015) evidenced the existence of two main lobes constituting the slide: one on the eastern side and the other on the western side, divided approximately by the Massalezza torrent (see Fig. 1). While sliding, the masses converged towards the center and behaved differently. In particular, in virtue of purely kinematic considerations based on photogrammetric images, Wolter et al. (2015) concluded that the western lobe (the one closer to the dam) experienced a lower roughness, and hence a lower resistance, and suggested that a four-sector zonation could better explain the behavior of the sliding mass. This constitutes a fundamental premise for our study.

The heterogeneity of the sliding surface in terms of friction angle was the object of previous analyses by the authors of this paper (Zaniboni et al. 2013; Zaniboni and Tinti 2014). Using a 1D block model, namely the code UBO-BLOCK1, the initial slide body was partitioned into six longitudinal sub-slides with approximately the same volume, and, correspondingly, the sliding surface was subdivided into six strips. By simulating the motion of each sub-slide, the objective was to find, for each strip, the friction angle that minimizes the discrepancy between the final position of the sub-slide and the observed deposit. The result was that the six strips could be grouped in a western and eastern region characterized by different friction coefficients, i.e. $\mu = 0.16$ and $\mu = 0.32$, respectively, corresponding to $\phi = 9°$ and $\phi = 17°$. The main limit of this approach was that each longitudinal strip was assumed to have a unique friction coefficient, which did not account for a possible uphill-downhill differentiation but only for east–west heterogeneity.

This result together with the most recent contributions appearing in the literature mentioned above encouraged us to study the friction angle zonation of the Vajont sliding surface by means of a more sophisticated numerical code, UBO-BLOCK2. This model is an extension of the code UBO-BLOCK1 from 1D to 2D. It approximates the moving mass with a mesh of interacting blocks that can change shape and height, but not volume. In opposition to all previous applications, here the heterogeneity of the sliding surface is explored, by subdividing it in an increasing number of zones (from one to four), investigating various levels of heterogeneity. Zone boundaries were selected a priori according to the literature. As a judging criterion for the accuracy of the simulation, we use an index of misfit measuring the discrepancy between the computed and observed deposit. We have found that a four-region partition with four distinct values of friction angle is the most suitable zonation since it provides the minimum misfit. Useful papers for establishing the explored zonations are the studies by Paronuzzi and Bolla (2012) and by Wolter et al. (2014), where the need for a heterogeneous sliding surface was highlighted.

The paper is structured as follows: a first part with the description of the numerical method, i.e. the 2D block model and the definition of the misfit index. Then, the data elaboration is presented, with a description of the slide geometry and of the sliding surface morphology. Afterwards, an illustration of the method adopted to evaluate the goodness of the zonations is presented, and, finally, a discussion of the results.

2. Numerical Techniques

2.1. Landslide Simulation Code: UBO-BLOCK2

Given the complexity of the landslide events, simulations are based on a number of simplifications. Our method belongs to the family of the lumped mass models, that was originally introduced by

approximating the slide to a single representative mass point (Hutchinson, 1986). Later, the model was extended by Hungr (1995), who described the mass as a set of distinct points. Hungr's approach is Lagrangian since the computational grid representing the body moves together with it during the motion, allowing a more convenient treatment of the motion equations.

Following this line of development, the model UBO-BLOCK2 makes a partition of the sliding mass into a number of "blocks" whose centers of mass (CoM) form the set of representative points mentioned above. The blocks are allowed to deform and change shape, but conserve their volume and cannot separate from—nor penetrate into—each other.

In a previous application to the Vajont slide, a 1D approach was used, implemented through the code UBO-BLOCK1 (see Zaniboni et al. 2013; Zaniboni and Tinti 2014), which is appropriate for landslides with significantly larger length than width. Since the Vajont slide does not fulfil this requirement, we divided it into six sub-slides with suitable aspect ratio (length/width $\gtrsim 3$), as mentioned in the introductory section, and examined their motion separately. In the 1D model, the mass is partitioned into a chain of blocks along the sliding direction, and all the CoMs are assumed to run down the same common path. The code requires that the CoM path and the lateral spreading of the landslide are defined a priori (see Tinti et al. 1997 for full details).

In the code UBO-BLOCK2, used in the present study, the sliding mass is divided into a 2D "mesh" of blocks with quadrilateral bases, interacting with the surrounding blocks (see Fig. 2 for a sketch of the block matrix of the Vajont landslide). Note that in the 2D case, the model does not need the a priori specification of a predefined trajectory for the block CoMs. The forces are evaluated for each CoM. The equations governing the slide motion can be expressed by:

$$\vec{a}_{i,k} = \vec{G}_{i,k} - \vec{R}_{i,k} + \vec{F}_{i,k} \qquad (1)$$

where $\vec{a}_{i,k}$ is the acceleration of the kth CoM of the mesh at the time t_i.

The acceleration in Eq. (1) is the sum of three main contributions:

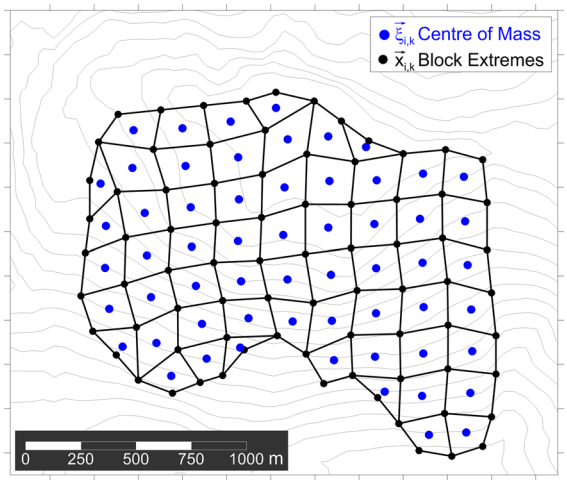

Figure 2
Sketch of the 2D mesh representing the 1963 Vajont sliding mass: CoMs (blue circles) and vertices (black circles) of the blocks basis. Their position, velocity and acceleration are computed at each time step, providing the full time history of the slide motion

- The gravitational term $\vec{G}_{i,k}$, including: (1) the effective gravity, that is the driving force, depending on the local slope; (2) the reaction force, depending on the local curvature and velocity; and (3) the buoyancy effect, if the mass moves in the water.
- The resistance term $\vec{R}_{i,k}$ accounting for: (1) the friction acting on the basal surface; (2) the interactions between the exposed surface of the sliding body and the environmental fluid that can be expressed in terms of tangential and frontal drag coefficients. If the landslide is subaerial, this latter term can be neglected.
- The internal interaction term $\vec{F}_{i,k}$ is the result of the mutual pushes and pulls between neighbor blocks during the motion. Modelling properly such behavior accounts for different types of sliding rheology. The model UBO-BLOCK2 accounts for mass stretching, with consequent change of shape, thickness and footprint area. It can simulate a slump-like motion where the total mass remains compact, as was the case of the Vajont slide.

The numerical resolution scheme for the core time loop of UBO-BLOCK2 is structured as follows:

- At time step i, the accelerations $\vec{a}_{i-1,k}$ are assumed to be known.

- From $\vec{a}_{i-1,k}$, the velocities $\vec{v}_{i,k}$ are obtained for all the CoMs by numerical integration.
- The velocities $\vec{v}^{ex}_{i,j}$ of the four vertices (or extremes) of each block base (black circles in Fig. 2) are obtained as a distance-weighted average of the surrounding CoMs (blue circles in Fig. 2). For the vertices lying on the slide boundary, this algorithm is properly modified, considering only the closest CoMs. Notice that the index j sweeps the set of the block vertices, while k sweeps the set of the block CoMs.
- The positions of the vertices $\vec{x}_{i,j}$ are computed by integration from the values of $\vec{x}_{i-1,j}$ and from their velocity $\vec{v}^{ex}_{i,j}$.
- From the positions of the block extremes, the CoM positions $\vec{\xi}_{i,k}$ are then calculated as a distance-weighted average of the positions of the surrounding vertices.
- At this stage, positions and velocities of all the reference points of the mass are completely determined. This enables one to evaluate all contributions included on the right-hand-side of Eq. (1), and consequently the accelerations $\vec{a}_{i,k}$. This computation is the final operation of the cycle, and allows one to proceed to the following time step $i + 1$.

In the code, the simulation continues as long as the average velocity of the landslide remains above a predefined threshold (below this small value, here fixed at 0.5 m/s, the dynamics is considered negligible and the simulation stops), or alternatively as long as none of the blocks experiences excessive deformation.

It is worth mentioning that the code UBO-BLOCK2 has been applied to study the tsunamigenic potential of submarine landslides in different environments. Some relevant cases are reported in Tinti et al. (2003, 2006), Argnani et al. (2011), Lo Iacono et al. (2012) and Argnani et al. (2012).

2.2. *Measuring the Simulation Accuracy: The Misfit Parameter*

The model parameters influence the sliding dynamics as well as the final shape of the simulated deposit. When data on the deposit are available, comparing observations with numerical results can be used to provide constraints on the values of the model parameters.

One way to assess the accuracy of a landslide simulation is to evaluate the discrepancy between two deposits, that is between two different mass distributions, say A and B, and to quantify their degree of overlapping. Denoting the volumes as V_A and V_B and the respective thicknesses as $H_A(x,y)$ and $H_B(x,y)$ over the space domain Γ, the normalized heights $h_A(x,y)$ and $h_B(x,y)$ are defined as:

$$h_A(x,y) = \frac{H_A(x,y)}{V_A}\Delta x \Delta y \tag{2a}$$

$$h_B(x,y) = \frac{H_B(x,y)}{V_B}\Delta x \Delta y \tag{2b}$$

Further, Δx and Δy represent the spatial resolution of the computational grid along x and y directions, respectively. Notice that the normalized heights h_A and h_B are thus dimensionless. The similarity index σ_{AB} can be defined through the following computational procedure: for each point of the domain $\Gamma(x,y)$, one takes the minimum value between $h_A(x,y)$ and $h_B(x,y)$ and then computes the space integral of such a minimum. For a discrete set of grid points, the resulting expression for σ_{AB} is:

$$\sigma_{AB} = \sum_{(x,y)\in\Gamma} \min[h_A(x,y), h_B(x,y)] \tag{3}$$

The misfit δ_{AB} is simply obtained as the complement to 1 of σ_{AB}, i.e. $\delta_{AB} = 1 - \sigma_{AB}$. The normalization introduced at the beginning guarantees that volume discrepancy is not accounted for. The comparison is done on the shapes and positions only: the closer the misfit is to zero, the more similar to each other they are.

In Fig. 3, a sketch of the procedure to calculate the misfit is shown. For graphical clarity, it is limited to a 1D representation: the two initial distribution thicknesses (upper panel) are depicted only along the x direction. The lower plot evidences the effect of normalization on the two curves, and the degree of overlapping measured by σ_{AB} is represented by the normalized area V_{AB} (marked by the hashed area). The bigger V_{AB} is with respect to the total area enclosed by the distributions A and B, and the more

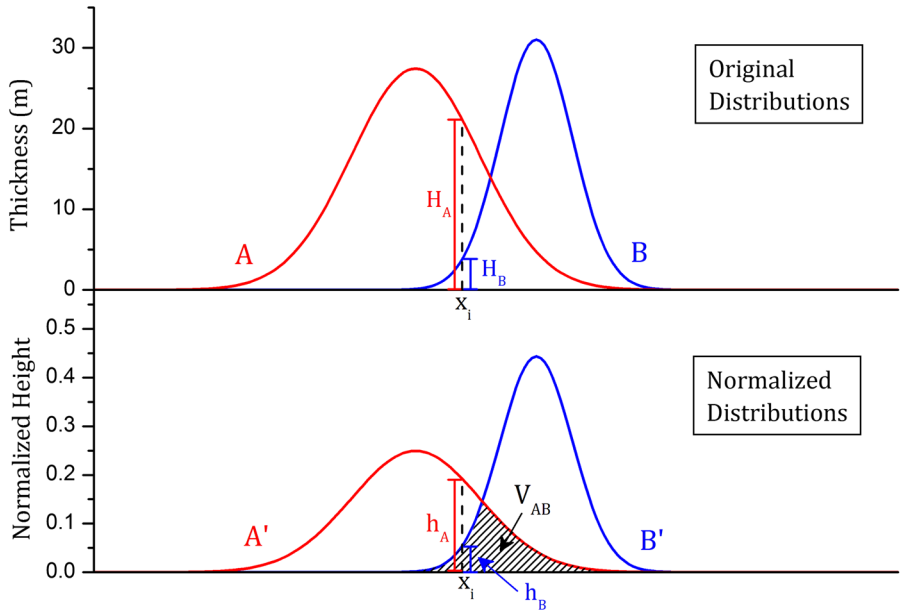

Figure 3
Similarity and misfit of two distributions, simplified along one single direction. Given A and B (red and blue lines, respectively, upper panel), they are normalized on the respective volumes (A' and B', lower panel). The difference of the area of overlapping V_{AB} (marked by the black diagonals) with respect to the total area enclosed by A and B is a measure of their similarity. The closer the value is to 1, the higher is the similarity between the two deposits, and the smaller is the misfit (see text for further explanations)

superimposed the two distributions are, the smaller the misfit is.

For more details on the misfit computation, see Appendix A in Zaniboni and Tinti (2014).

3. *Reconstructed Morphology and Discretization of the Vajont Slide*

In order to run the code and simulate the 1963 Vajont slide movement, an accurate reconstruction of the sliding surface and sliding mass morphology is needed. The procedure we adopted is described in details in Zaniboni and Tinti (2014) regarding the 1D block model.

It is worth mentioning here that the sliding surface follows the profiles suggested by Selli and Trevisan (1964) and accepted by Hendron and Patton (1985) for the reconstruction of the hidden depleted area, i.e. the part that was covered by the mass before the slide and that remained beneath the deposit at the end of the motion. The result is that the western portion of the sliding surface is characterized by a chair-like slope (steep uphill—almost flat in the valley bottom). Instead, to the east, the profile is parabolic. The remaining part of the sliding surface is obtained from the geological maps (Rossi and Semenza 1965). From our reconstruction, the initial involved mass results in about 258 million m^3.

The initial body, represented by means of a regular grid with resolution of 20 m, has been discretized into a mesh of 59 elements with typical side length of about 200 m (blue grid of Fig. 4) entailing as many as 79 vertices. This configuration is a good compromise between the need to characterize the mass in the most accurate way and the amount of time required to run the model. We observe that this discretization introduces a small but inevitable bias: if we compute the misfit between the reconstructed initial mass and the corresponding discretized body, we get a value of 0.06, certainly low but not negligible, and that will affect the final comparison between the observed and simulated deposits.

4. *Zonation of the Sliding Surface*

The first studies on the Vajont slide assumed that the sliding surface was well defined with a homogeneous friction coefficient. Later studies supported this

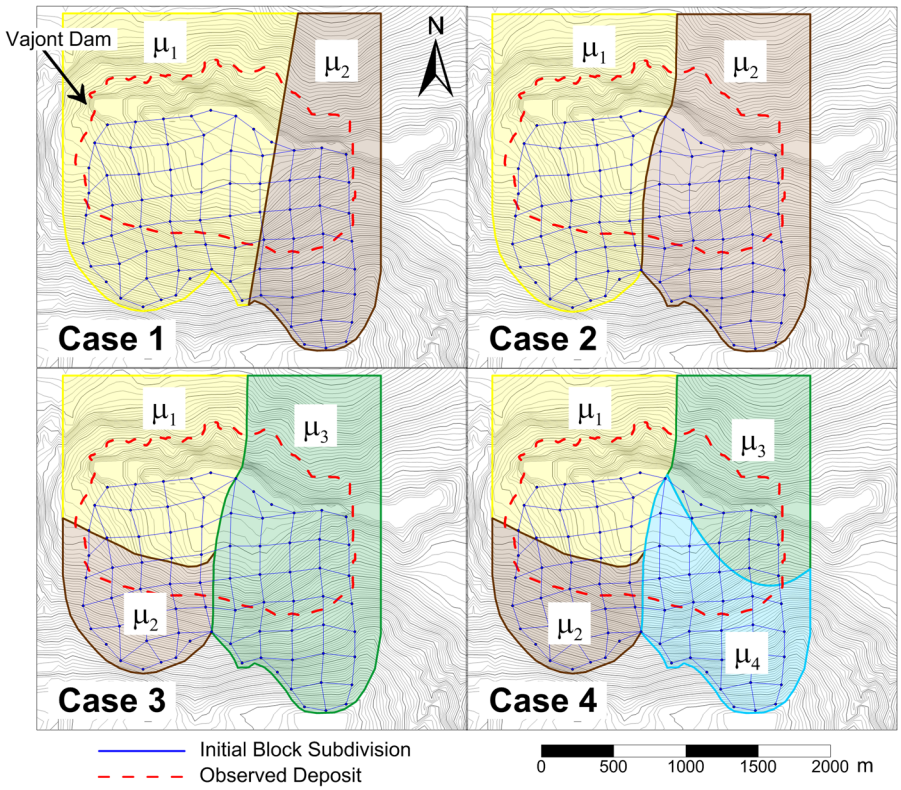

Figure 4
Zonations of the sliding surface analyzed in this study. The blue mesh marks the initial block subdivision; the red dashed line is for the boundary of the observed deposit

hypothesis (Hendron and Patton 1985; Superchi 2012), so that at a certain point, there was a general agreement that the sliding surface was mainly composed of clay, though more complex or chaotic formations were suggested in some areas (Paronuzzi and Bolla 2012). For example, Selli and Trevisan (1964) hypothesized that the sliding surface was different in the easternmost corner downhill, since they believed that the failure surface went deeper, involving also layers underneath the main clay layer forming the surface elsewhere. Recently, the issue of the sliding surface zonation has attracted more attention and different views have been advanced. A different two-zone surface was conjectured by Superchi (2012) and by Bistacchi et al. (2013), who fixed a boundary along the depression dug by the Massalezza torrent, and speculated that the two lobes moved separately. Later, a four-block zonation was credited by Wolter et al. (2014, 2015), implying more complex sliding dynamics.

The present study aims at providing a contribution to the debated issue of the sliding surface zonation. In our numerical simulations, all the complexities about the sliding surface shape and heterogeneity are simplified by assuming a well-defined sliding surface geometry, not changing during the motion. The slip surface is partitioned into domains characterized by their own basal friction coefficient $\mu = \tan\phi$ (with ϕ friction angle).

The homogeneous case is investigated first (here named as case 0), and then heterogeneous cases up to a maximum number of four zones. The first heterogeneous configuration (case 1, Fig. 4) assumes two zones. Assuming the same zonation we found with a 1D model (Zaniboni and Tinti 2014), the analysis is repeated here by means of the 2D model. Case 2 is still based on a two μ sectors, but the boundary between the zones runs approximately along the Massalezza torrent, following the suggestion by Superchi (2012) and the two-lobes hypothesis by Bistacchi et al. (2013).

Case 3 (Fig. 4) has been conceived as a refinement of case 2: the western zone is split in two parts, one at higher elevation and the other in the valley bottom, while the eastern portion remains unchanged. In this way, one can test the different behavior of the uphill and downhill portions of the western part of the sliding surface.

Case 4 is a four-area zonation differentiating west from east and uphill from downhill, which approximates the four-sector hypothesis advanced by Wolter et al. (2015). The boundaries of the zonation areas are portrayed in Fig. 4.

Analyzing a configuration with N zones implies exploring an N-dimensional space of parameters (μ_1, μ_2,…, μ_N). If one discretizes each interval of μ_i with M points, the number of possible combinations of μ values, and thus the number of required simulations, is M^N, which becomes a serious computational demand as N increases.

5. Searching for the Best Configuration: Results and Discussion

5.1. The Homogeneous Case

As a starting case (case 0), we first adopt a homogeneous friction coefficient, which is an assumption often made by numerical modelers who focus on the landslide and water flow dynamics (e.g. Sitar et al. 2005; Crosta et al. 2016; Zhao et al. 2016). The investigated range for the μ values extends from 0.0 to 0.50, with a step of 0.01. For each value of the friction coefficient, the landslide motion is simulated with the model UBO-BLOCK2, and the misfit between the numerical and observed deposits is computed following the procedure described in Sect. 2.2 (with A and B denoting the two mass distributions, respectively). Results are plotted through the misfit curve of Fig. 5 (black triangles), showing a clear minimum around $\mu = 0.21 - 0.22$, where the misfit is about 0.125. Higher and lower μ result in bigger differences. Values of μ assumed in previous studies (summarized in Table 1, and marked by red circles in Fig. 5) are superimposed on the misfit curve. It is surprising to see how close the value of 0.236 derived by Ciabatti (1964) is to the best cases, on the basis of very crude considerations. It is worth observing that Hendron and Patton (1985), Sitar et al. (2005) and Alonso and Pinyol (2010) took the value $\mu \approx 0.21$ in their study that perfectly overlaps with the minimum of Fig. 5. Other works, such as the first estimations by Hendron and Patton (1985), Crosta et al. (2016) and Zhao et al. (2016), selected lower values (0.10 and 0.17), that, however, according to our simulations, imply significant discrepancies with observations.

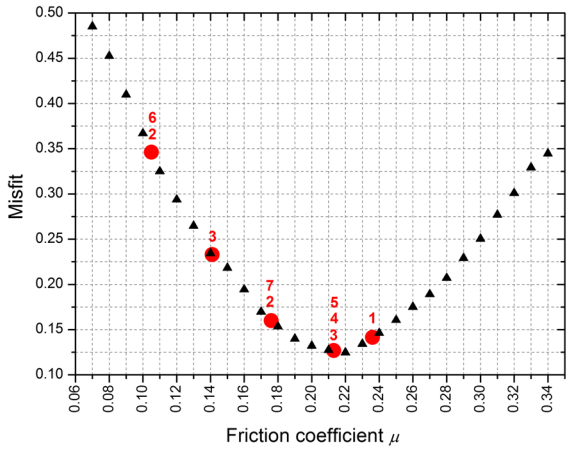

Figure 5
Misfit curve for a homogeneous sliding surface. The red circles and numbers mark the μ values adopted in previous works by other authors (see reported references in Table 1). The black triangles indicate the misfit obtained applying UBO-BLOCK2 code with different values of μ

Table 1

Friction coefficients μ and corresponding friction angles ϕ for a homogeneous sliding surface

#	Citation	ϕ (°)	μ	Misfit
1	Ciabatti (1964)		0.236	0.1415
2	Hendron and Patton (1985)	6–12	0.105–0.213	0.3462–0.1268
3	Semenza and Ghirotti (2000)	8–12	0.141–0.213	0.2329–0.1268
4	Sitar et al. (2005)	12	0.213	0.1268
5	Alonso and Pinyol (2010)	12	0.213	0.1268
6	Crosta et al. (2016)	6	0.105	0.3462
7	Zhao et al. (2016)	10	0.176	0.1600

Misfit values from literature are computed by interpolation from the misfit curve of Fig. 5

5.2. Heterogeneous Cases

As regards the heterogeneous cases, for each of the sliding surface configurations reported in Fig. 4, the investigation on the friction coefficient values proceeded as follows:

- Selecting the μ_i combination, that is the μ_i values for each zone i of the sliding surface;
- Running the simulation through the code UBO-BLOCK2;
- Calculating the misfit parameter.

This procedure has been repeated for all possible combinations of the friction coefficients for the different zones, by varying μ_i in the range 0.00–0.50 at a 0.01 step. For the 2-zone cases, this entails as many as 2601 simulations. When the zones are 3 or 4, this number grows to over 130,000 and to more than 6 million respectively. In these latter cases, the strategy was to investigate the values of μ with a higher step (0.02 and 0.033 in three- and four-zone configurations, respectively), searching for a reasonable compromise between the total number of simulations (i.e. the computational time) and the accuracy of the analysis.

In simulations with low friction coefficients, the slide might climb up the opposite flank of the Vajont valley, reverse the motion and then come back towards the valley bottom: no evidence of any backward motion of the failure mass was found in the Vajont post-slide surveys. Consequently, all μ combinations resulting in such a motion have been discarded and the respective misfit value has not been considered.

Coming to the results of the simulations, Fig. 6 provides a good view of the misfit distribution for the two-area configurations, i.e. case 1 and case 2. Each point of the plane (μ_1, μ_2) reports the value of the corresponding misfit according to a color scale. For case 1, the best combination is provided by $\mu_1 = 0.17$ and $\mu_2 = 0.34$ (cyan star in Fig. 6, left panel; see also Table 2), and, considering the area with the smallest values (purple circles), μ_1 is in the interval 0.17–0.20 and μ_2 in the interval 0.29–0.36. In case 2, the lowest misfit is found for $\mu_1 = 0.14$ and $\mu_2 = 0.29$ (cyan star in the right panel of Fig. 6; Table 2), with μ_2 in the interval 0.29-0.36 and μ_1 between 0.08 and 0.18. Such findings confirm the results obtained with the 1D model (Zaniboni and Tinti 2014), i.e. that the

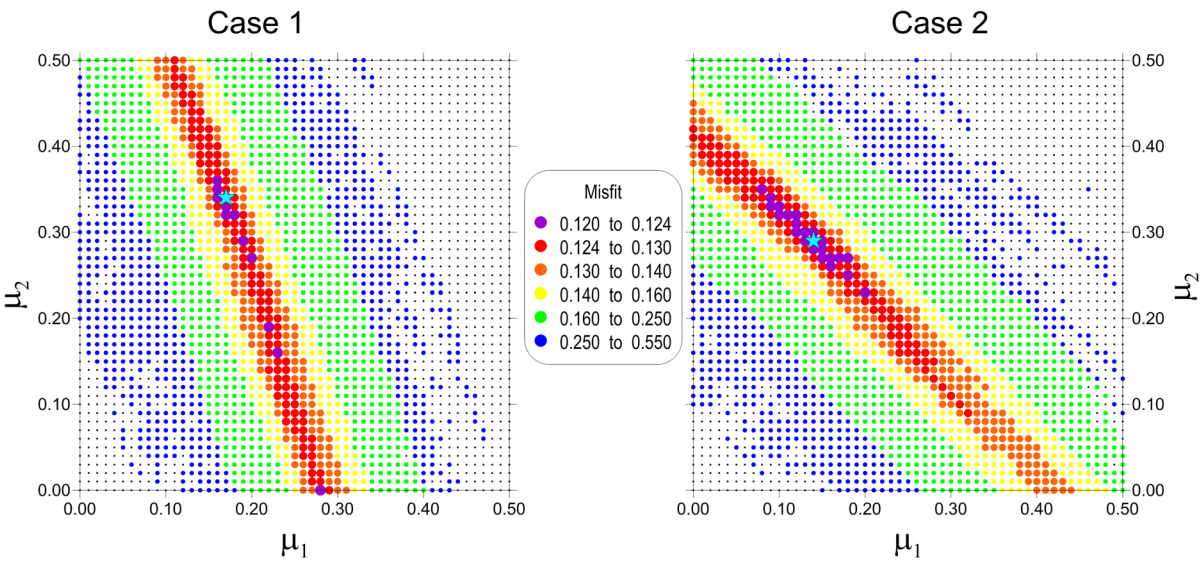

Figure 6
Misfit distributions of two-sector zonations (cases 1 and 2 of Fig. 4). In a (μ1, μ2), space misfits are marked by solid circles. Purple circles mark the lowest values, and for the more accurate simulations, blue circles mark the highest. The black points mark simulations with reverse motion, that are then discarded. The cyan star evidences the combination providing the minimum misfit

Table 2

Misfit (δ) and friction coefficients estimated for the zonations analyzed in the paper. On the left side of the table ("best case" column), the combination of μ values providing the least misfit are reported

Case 0 (homogeneous, μ step = 0.01, N_{tot} = 51)		
Best case		
μ = 0.22	δ = 0.1248	
Case 1 (heterogeneous, 2 zones, μ step = 0.01, N_{tot} = 2601)		
Best case		Selected set (N_{SEL}= 118)
μ_1 = 0.17	δ = 0.1213	μ_1 = 0.194 ± 0.039
μ_2 = 0.34		μ_2 = 0.256 ± 0.122
Case 2 (heterogeneous, 2 zones, μ step = 0.01, N_{tot} = 2601)		
Best case		Selected set (N_{SEL}= 100)
μ_1 = 0.14	δ = 0.1211	μ_1 = 0.134 ± 0.066
μ_2 = 0.29		μ_2 = 0.287 ± 0.065
Case 3 (heterogeneous, 3 zones, μ step = 0.02, N_{tot} = 17,576)		
Best case		Selected set (N_{SEL}= 785)
μ_1 = 0.12	δ = 0.1199	μ_1 = 0.137 ± 0.073
μ_2 = 0.24		μ_2 = 0.201 ± 0.114
μ_3 = 0.28		μ_3 = 0.254 ± 0.059
Case 4 (heterogeneous, 4 zones, μ step = 0.033, N_{tot} = 65,536)		
Best case		Selected set (N_{SEL} = 3761)
μ_1 = 0.1	δ = 0.1188	μ_1 = 0.140 ± 0.073
μ_2 = 0.3		μ_2 = 0.198 ± 0.116
μ_3 = 0.233		μ_3 = 0.263 ± 0.116
μ_3 = 0.3		μ_4 = 0.233 ± 0.085

N_{tot} stands for the total number of simulations performed. The columns on the right report the statistical analysis of the results for the "selected set", (i.e. the N_{SEL} combinations providing misfit below 0.13). The shown values for the friction coefficient are given by the 50th percentile (the median of the μ frequency distribution). The associated uncertainty, quantifying the spread around the median, is computed as half of the difference between the 25th and the 75th percentiles

friction coefficient on the west side is smaller than on the east.

5.3. Statistical Analysis

For a 3-area zonation, the number of simulations needed to cover the friction coefficient interval 0.00–0.50 with a 0.02 step is 17,576. Observe that the three-parameter misfit distribution cannot be conveniently represented in a plane as in Fig. 6. Hence, a different method of interpretation and representation has been adopted, according to the following scheme:

- selecting the subset of the "best combinations" of friction coefficients, denoted hereafter as "selected set", that is defined as the combinations providing a misfit lower than a given threshold (taken here as 0.13, a value providing 785 suitable configurations, sufficient to perform a statistical analysis);
- Computing the frequency distribution of each μ_i among the selected set;
- Taking the median (50th percentile) as the representative value of the friction coefficient. The difference between the 25th and 75th percentiles indicates how much the selected set spreads around the median; the spread divided by two is used to define the uncertainty interval (Table 2).

This kind of analysis provides indications on the most recurring values of friction coefficient along the best configurations. Table 2 and Fig. 7 summarize the results that are given also for the two-sector zonations (cases 1 and 2). In general, in the west, the friction coefficient is smaller than in the east. For case 1, frequency distributions of Fig. 7 are quite different: for μ_1, it is peaked and narrow, while for μ_2, it is flat. Using percentiles, it follows that μ_1 is 0.19 with an uncertainty interval of ± 0.04, and μ_2 is 0.25 with a wider spread (around 0.23). Indeed, the flatness (or uniformity) of the μ_2 distribution suggests that the slide motion is mainly determined by the value of μ_1, since changing μ_2 influences the misfit less. This is probably due to the different extents of the two zones, zone 1 being much larger than zone 2.

In case 2, instead, zones 1 and 2 have comparable dimensions. The two distributions turn out to be similar (right upper panel, Fig. 7), but centered on different values, namely 0.13 for μ_1 and 0.29 for μ_2, with spread equal to 0.13 for both.

The three-sector zonation (case 3) provides an improvement on the misfit value, that goes below 0.12 in the best case. The combinations with misfit below the 0.13 threshold (i.e. of the selected set) are 785 (about 4% of the total). The frequency distributions show a concentration of values around 0.14 and 0.25 for zones 1 and 3 with estimated uncertainties of 0.07 and 0.06, respectively (lower-left panel of Fig. 7). As regards μ_2, the distribution has an almost linear decreasing trend, with a median of 0.20 and a large spread of 0.23. This seems to suggest a low friction in the western valley bottom (zone 1) and a high friction on the eastern side (zone 3). The upper western part (zone 2) has an intermediate value, but

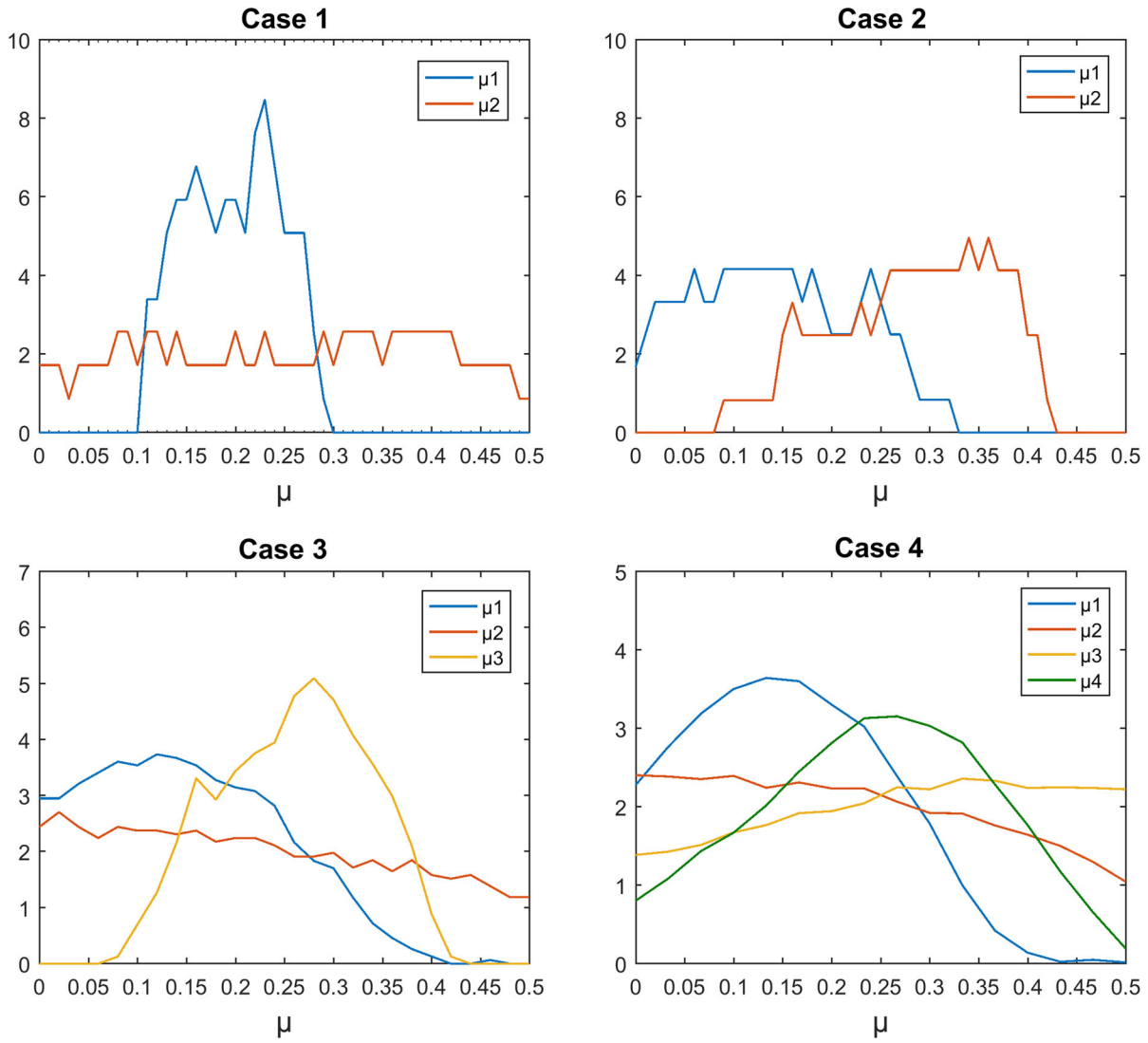

Figure 7
Frequency distributions of μ for the examined heterogeneous zonations. Only combinations entering the selected set (i.e. with associated misfit less than 0.13) contribute to the analysis

the high variability of the values entering the selected set suggests that its influence to the slide motion is small.

A further improvement is the division of the eastern section into up- and down-hill areas, in order to assess the respective influence on the dynamics (four-sector case). In order to cover the whole domain, 0.00–0.50, of the friction coefficient values, saving together computational time, steps of 0.033 have been considered. This led to about 65,000 possible combinations. Among these, as many as 3761 (over 5% of the total) give misfit values less than 0.13 and contribute data to the frequency distributions that are portrayed in the lower right panel of Fig. 7. The μ_1 and μ_4 distribution (zones in the western bottom and eastern uphill, respectively) show peaks at about 0.14 and 0.23 (Table 2), while the other curves are like an almost flat concave parabola with the vertex on the left (μ_2, orange) and on the right (μ_3, green). This implies that the corresponding medians are 0.20 and 0.23, but the associated uncertainty intervals are very large

($\pm$ 0.116 as reported in Table 2). The conclusion is that the friction coefficient in zone 1 (valley bottom close to the dam) is low, and it is high in zone 4 (uphill east), that is in an area where an additional friction was hypothesized by Hendron and Patton (1985) due to the supposed influence of lateral faulting. Instead, in zones 2 and 3, the value of μ is intermediate, but cannot be determined properly since the distributions are rather flat. This means that the slide dynamics here is somewhat insensitive to the values of the friction angle.

6. *The Vajont Slide Dynamics*

From the misfit values analysis, one may observe that many configurations lead to a final deposit fitting well with the observed one. Looking at the best misfit values of Table 2, one sees that they are all around 0.12. Considering that part of the discrepancy (about 6%) is due to the slide discretization into blocks (see Sect. 3), the misfit ascribable to the dynamics is the remaining 6%. Zonations with increasing heterogeneity lead to decreasing misfits, but the misfit reduction is in the order of 0.5% (from 0.1254 to 0.1188). Nonetheless, we believe that this improvement is significant to provide hints on the value of the zonation.

In this section, we only present the results of the configuration that leads to the best solution: they refer to the combination of friction coefficients of the four-sector zonation providing the least misfit among all the examined scenarios, i.e. 0.1188 (see Table 2, case 4). Figure 8 shows the path followed by the nodes forming the vertices of the blocks, that is $\vec{x}_{i,j}$ (black circles). The simulation confirms that on sliding

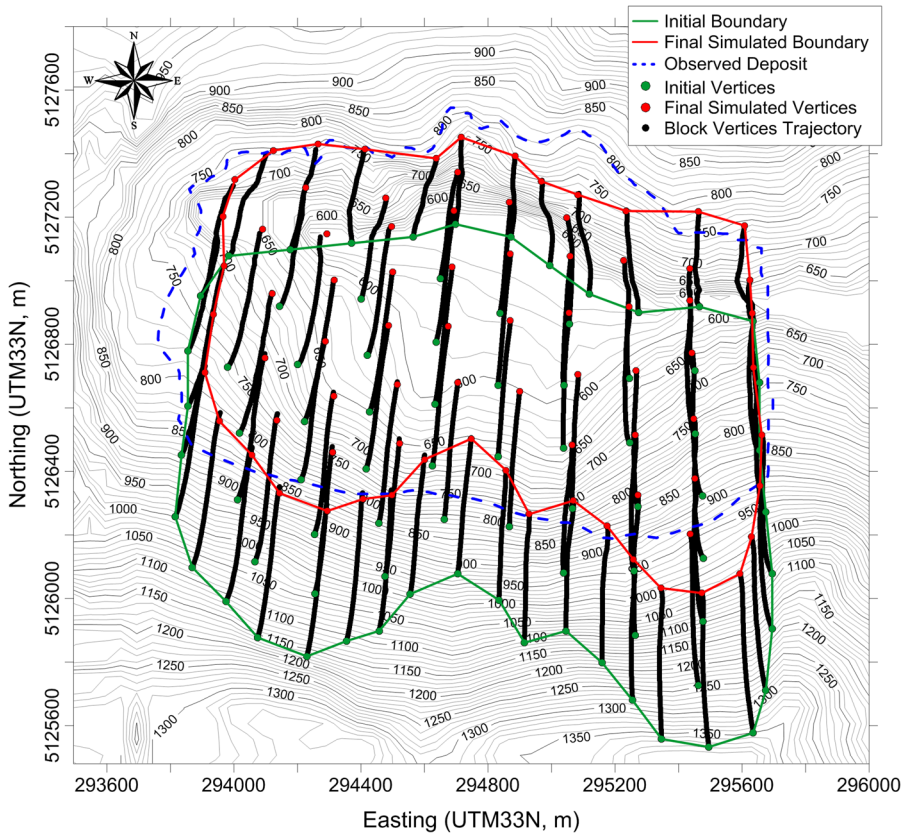

Figure 8
Trajectories (black lines) of the block vertices from the initial configuration (green points and boundary) to the final position (red points and boundary). The blue dashed contour is the observed deposit. Notice the eastward deviation of the western blocks and the opposite behavior of the eastern ones

down, (1) the mass converges towards the central part of the valley, since (2) the western lobe deviates slightly eastward and the eastern lobe deviates westward (see Bistacchi et al. 2013), and (3) the deviation is more pronounced uphill (as seen in Wolter et al. 2015). We remark that this is compatible also with considerations found in Superchi (2012) and with simulations by Crosta et al. (2016).

The simulated deposit footprint (red boundary) fits the observations (dashed blue line) satisfactorily, though with discrepancies in some regions. The uphill part of the simulated deposit follows the observed boundary only roughly. It remains at higher altitude in the east and west, and slides more downhill in the center. The slide fronts overlap better, but in the central part, the simulated front climbs up the opposite side of the valley less than observed. The discrepancies are probably due to a limitation of the code, that is unable to reconstruct properly the complex deformation and dilation of the sliding body, especially because it does not account for overthrust and forming of internal surfaces.

The numerical code, in addition to the final shape of the deposit, provides the full time history of the motion of all representative points (CoMs and block basis vertices). Figure 9 reports some kinematic variables: W–E components (right panels) and S–N (left panels). It is easy to see that most of the motion occurred along the S–N direction.

Considering the velocity time history, one notices that the S–N component of the average velocity of the slide, i.e. the average velocity of the block CoMs,

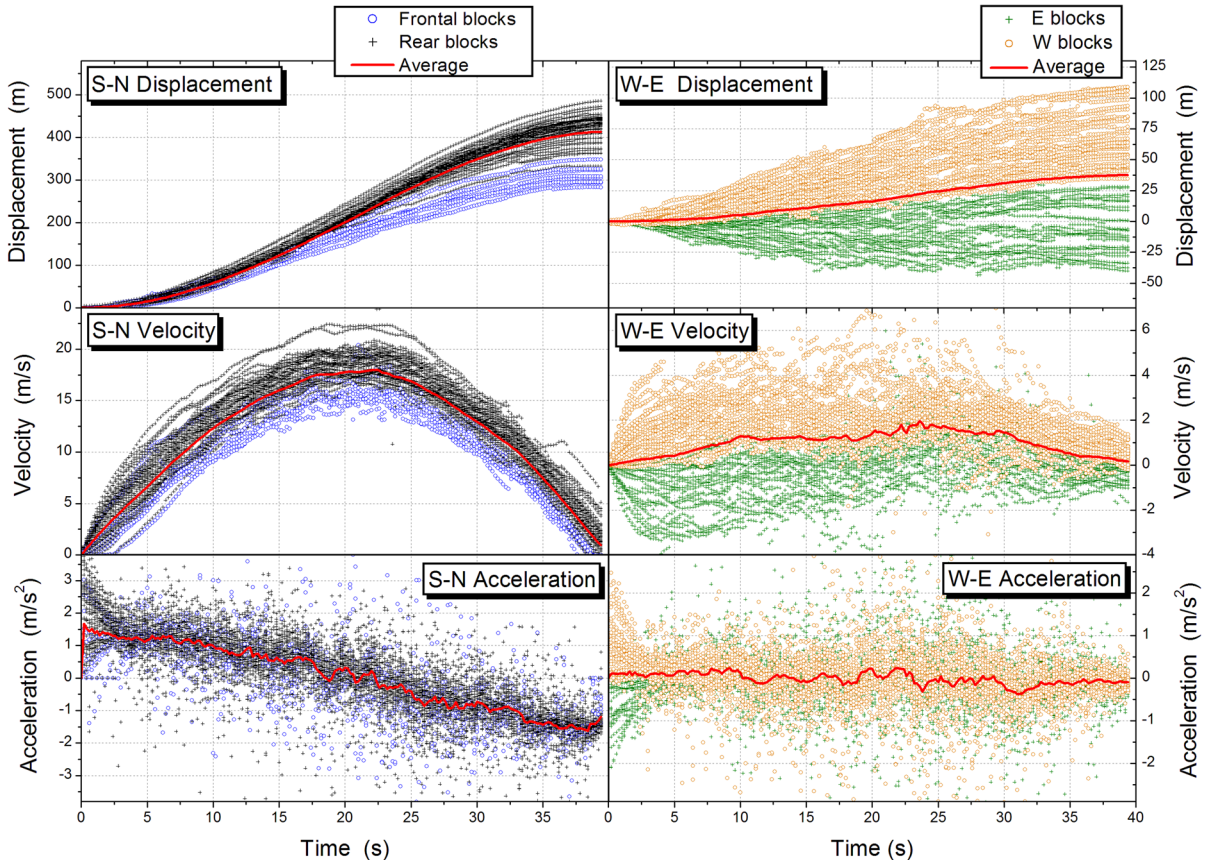

Figure 9
Vajont landslide kinematics, decomposed along S–N (left panels) and W–E (right panels) directions. The 1963 motion was mainly from S to N. In the S–N graphs, the front blocks located in the valley bottom are marked by blue points; the rear blocks, in the head region, by the black circles. In the W–E graphs, the blocks located west of the Massalezza torrent are in orange and the eastern ones in green. In all graphs, red lines mark the weighted average quantity, where the average is over all CoMs and weights are the volume blocks

attains a peak value slightly more than 17 m/s after 20 s, while the E–W component remains below 2 m/s. Moreover, the values obtained for the velocity as well as the motion duration (40 s) fit very well the observations and agree with the reconstructions mentioned before, including the recent work by Dykes and Bromhead (2018b) quantifying the motion duration as 30–45 s.

The velocity plot shows other interesting characteristics of the motion. The S–N velocities of the frontal blocks (in blue), initially located in the valley bottom on a gentler slope, are systematically smaller than the velocities of the rear blocks (in black), with peak values of 15 m/s vs. 20 m/s. In addition, the S–N displacement graph shows that front blocks move less than the average, i.e. about 300 m vs. 400 m (in agreement with the observations by Selli and Trevisan 1964, and by Ciabatti 1964), meaning that the mass compresses at the valley bottom.

The W–E graphs of Fig. 9 distinguish between the CoM belonging to the western lobe (in orange) and the eastern lobe (in green), divided roughly by the Massalezza torrent. The displacement graph shows a clear distinction between the western and the eastern CoMs: for the former, positive values are found, corresponding to an eastward motion of almost 100 m; for the latter, mainly negative values up to 30 m can be noticed, evidencing a concentration towards the Massalezza incision, somewhat similar to the two-lobe behavior envisaged by Bistacchi et al. (2013). The average displacement (red line) shows a prevailing eastern deviation of the whole mass, consistent with Hendron and Patton's (1985) findings. The velocity plot confirms the same feature, with a prevailing eastward deviation of the sliding motion, and general higher values for the western blocks than for the eastern ones, accounting for different sliding surface shape and friction coefficient values.

From the acceleration plots, it is less easy to extract information, due to the very scattered and sparse instantaneous values, probably due to the reciprocal forces of the blocks during the descent. The average trend (red line) shows a positive initial (and maximum) S–N acceleration attaining values of 1.6 m/s^2, compatible with values hypothesized by Ciabatti (1964), and three times higher than the results from Ward and Day (2011). The transversal acceleration, apart from an initial clear distinction between the western CoMs (positive, i.e. moving eastward), and the eastern ones (negative, i.e. going westward), ranges around zero with some oscillations, especially in the central phase, when the slide begins to decelerate and the interaction forces prevail but balance each other as an overall effect.

7. Conclusions

This paper follows a research line that was started by the authors in previous works, and speculates that the interaction between the landslide bottom and the sliding surface was the key factor leading to the observed differential kinematics for the Vajont event. Coherently, this means that, among the many parameters governing the motion of the landslide in numerical simulations, focus has to be put on the bottom friction, and that numerical modelling can be used as an investigation tool to determine possible different bottom friction patches on the sliding surface.

The main results of our analyses can be summarized as follows:

1. When assuming a constant friction coefficient (case 0), we find that the best estimate for μ is between 0.21 and 0.22. This is consistent with previous analyses (e.g. Ciabatti 1964). This seems a sort of average value: indeed, when comparing it to the results of the heterogeneous zonations, it turns out to be intermediate between the highest and smallest values.
2. Case 1 and case 2 examine two-sector zonations. Case 1 has the same partition resulting from the paper by Zaniboni and Tinti (2014), while case 2 examines a partition with a boundary along the Massalezza torrent (as in Bistacchi et al. 2013). Both zonations are an improvement of the homogenous case, but frequency distributions of μ_1 and μ_2 are different (Fig. 7). For case 1, the extent of sector 2 is too small compared to sector 1, and the motion of the slide is scarcely influenced by its friction coefficient. The consequence is that the only relevant friction coefficient, i.e.μ_1, takes a value similar to the

homogeneous case, while the other is practically undetermined (uniform distribution). On the contrary, for case 2, the distribution graphs discriminate quite well between a smaller μ_1 and a larger μ_2.

3. Case 3 has no counterpart in the known literature and is examined here for the sake of completeness. The case confirms the substantial difference between the eastern and the western lobes and shows also that subdividing the second in upper and lower sectors entails that one of them (in this case, the lower one) has a predominant role in governing the landslide motion. In fact, the distribution of μ_2 (upper western sector) is not far from being uniform.
4. Case 4 turns out to be the master case. The four-sector zonation, following the work by Wolter et al. (2014), provides the best results in terms of deposit misfit. It proves that sector 1 (west downhill) and sector 4 (east uphill) are the ones prevailing in determining the motion (unimodal peaked distributions) and that μ_4 is substantially larger than μ_1. As regards the other sectors, sector 3 on the east has a roughness coefficient somewhat larger than sector 2 on the west, but distributions are close to flatness and so do not possess discriminating power.
5. The general analysis shows that the Vajont landslide had a dynamic behavior that can be justified in terms of heterogeneity of the friction coefficients of the sliding surface. Indeed, the friction coefficient used in the numerical models can be seen as a parametrization of the complex interaction process between the base of the mobilized mass and the top of the rock body constituting the sliding surface. This study shows that the processes most influential for the motion occurred in the head region to the east of the Massalezza torrent and in the toe region to the west (sectors 4 and 1 of case 4, respectively).
6. The resulting dynamics fits very well the observations and the outputs of previous applications of numerical codes. The motion duration is about 37 s and the maximum velocity reaches 18 m/s, with a differentiation between the rear portion (up to 20 m/s) and the frontal one (around 15 m/s). The initial acceleration results in about 1.6 m/s^2, in good agreement with values found in literature (see e.g. Dykes and Bromhead, 2018a and references therein).
7. The results reported here are obtained by means of a code that assumes simplifications in the morphology setting and in the landslide dynamics and that therefore does not require huge computational effort. Thus, it allows one to run tens of thousands of cases in a reasonable time. Exploration of more complicated zonations (number of zones larger than four) would imply to increase the number of cases by one or more orders of magnitude. Nonetheless, it is possible to quantify the effects of the different portions of the sliding surface on the dynamics, highlighting some interesting aspects of the Vajont landslide.
8. It is worth stressing that our analysis is more adequate for a post-disaster study than for an emergency crisis. Indeed, in the presence of a potential collapse, the assumption of a homogenous sliding surface might provide an acceptable first esteem of the slide motion (see Ciabatti 1964, for the Vajont landslide). However, further refinements could provide more adequate and realistic pictures of the slide dynamics.
9. The heterogeneity highlighted here pertains to the sliding process, but one can speculate that it is also related to the process leading to mass instability. In other terms, one can figure out that dynamic friction coefficient zonations correspond to equivalent zonations of the static friction coefficients. This issue cannot be explored with the tool used in this study, that is by modelling the landslide motion. Rather, it can be investigated through a stability analysis and is the object of an ongoing research taking into account the whole recent history of the Mt. Toc flank (see Paparo et al. 2013 for preliminary results).
10. Future improvements of this work could be the investigation on the assumption of different geometries of the sliding surface, as postulated by Bistacchi et al. (2013) and by Dykes and Bromhead (2018a), and on the related influence on the results reported here.

Acknowledgements

The authors are indebted to the reviewers, one anonymous and the other Dr. Rachid Omira, who contributed to the improvement and robustness of the manuscript.

References

Alonso, E. E., & Pinyol, N. M. (2010). Criteria for rapid sliding I. A review of Vaiont case. *Engineering Geology, 114*(2010), 198–210. https://doi.org/10.1016/j.enggeo.2010.04.018.

Argnani, A., Armigliato, A., Pagnoni, G., Zaniboni, F., Tinti, S., Bonazzi, & C. (2012). Active tectonics along the submarine slope of south-eastern Sicily and the source of the 11 January 1693 earthquake and tsunami. *Natural Hazards and Earth System Sciences*, *12*, 1311–1319. http://www.nat-hazards-earth-syst-sci.net/12/1311/2012/, https://doi.org/10.5194/nhess-12-1311-2012.

Argnani, A., Tinti, S., Zaniboni, F., Pagnoni, G., Armigliato, A., Panetta, D., et al. (2011). The eastern slope of the southern Adriatic basin: a case study of submarine landslide characterization and tsunamigenic potential assessment. *Marine Geophysical Researches, 2011*(32), 299–311. https://doi.org/10.1007/s11001-011-9131-3.

Bistacchi, A., Massironi, M., Superchi, L., Zorzi, L., Francese, R., Giorgi, M., Chistolini, F., & Genevois, R. (2013). A 3d geological model of the 1963 Vajont landslide. *Italian Journal of Engineering Geology and Environment Book Series* (6), © 2013 Sapienza Università Editrice. https://doi.org/10.4408/ijege.2013-06.b-51.

Caloi, P. (1966). L'evento del Vajont nei suoi aspetti geodinamici. *Annali di Geofisica, XIX*, 1–74 **(in Italian)**.

Carloni, G.C., & Mazzanti, R. (1964). Rilevamento geologico della frana del Vajont. *Giornale di Geologia, Annali del Museo Geologico di Bologna, XXXII*, 105–123 **(in Italian)**.

Cecinato, F., Zervos, A., & Veveakis, E. (2011). A thermo-mechanical model for the catastrophic collapse of large landslides. *International Journal for Numerical and Analytical Methods in Geomechanics, 35,* 1507–1535. https://doi.org/10.1002/nag.963.

Ciabatti, M. (1964). La dinamica della frana del Vajont. *Giornale di Geologia, Annali del Museo Geologico di Bologna, XXXII*, 139–153 **(in Italian)**.

Crosta, G. B., Imposimato, S., & Roddeman, D. (2016). Landslide spreading, impulse water waves and modelling of the Vajont Rockslide. *Rock Mechanics and Rock Engineering*. https://doi.org/10.1007/s00603-015-0769-z.

Del Ventisette, C., Gigli, G., Bonini, M., Corti, G., Montanari, D., Santoro, S., et al. (2015). Insights from analogue modelling into the deformation mechanism of the Vaiont landslide. *Geomorphology, 228,* 52–59. https://doi.org/10.1016/j.geomorph.2014.08.024.

Dykes A. P., & Bromhead, E. N. (2018a), The Vaiont landslide: re-assessment of the evidence leads to rejection of the consensus. *Landslides*. https://doi.org/10.1007/s10346-018-0996-y.

Dykes A. P., & Bromhead, E.N. (2018b), New, simplified and improved interpretation of the Vaiont landslide mechanics. *Landslides*. https://doi.org/10.1007/s10346-018-0998-9.

Ferri, F., Di Toro, G., Hirose, T., Han, R., Noda, H., Shimamoto, T., et al. (2011). Low- to high-velocity frictional properties of the clay-rich gouges from the slipping zone of the 1963 Vaiont slide, northern Italy. *Journal of Geophysical Research, 116,* B09208. https://doi.org/10.1029/2011JB008338.

Genevois, R., & Ghirotti, M. (2005). The 1963 Vaiont landslide. *Giornale di Geologia Applicata, 1,* 41–52. https://doi.org/10.1474/GGA.2005-01.0-05.0005.

Hendron, A. J., & Patton, F.D. (1985). The Vajont slide, a geotechnical analysis based on new geological observations of the failure surface. Technical report GL85-5, US Army Corps of Engineers Waterways Experiment Station, Vicksburg, (2 volumes).

Hungr, O. (1995). A model for the runout analysis of rapid flow slides, debris flows, and avalanches. *Canadian Geotechnical Journal, 32,* 610–623.

Hutchinson, J. N. (1986). A sliding-consolidation model for flow slides. *Canadian Geotechnical Journal, 23,* 663–677.

Kilburn, C. R. J., & Petley, D. N. (2003). Forecasting giant, catastrophic slope collapse: lessons from Vajont, Northern Italy. *Geomorphology, 54,* 21–32. https://doi.org/10.1016/S0169-555X(03)00052-7.

Lo Iacono, C., Gràcia, E., Zaniboni, F., Pagnoni, G., Tinti, S., Bartolomé, R., et al. (2012). Large, deepwater slope failures: Implications for landslide-generated tsunamis. *Geology, 40*(10), 931–934. https://doi.org/10.1130/G33446.1.

Mantovani, F., & Vita-Finzi, C. (2003). Neotectonics of the Vajont dam site. *Geomorphology, 54,* 33–37. https://doi.org/10.1016/S0169-555X(03)00053-9.

Paparo, M. A., Zaniboni, F., & Tinti S. (2013). The Vajont landslide, 9th October 1963: Limit equilibrium model for slope stability analysis through the Minimum Lithostatic Deviation method. *Italian Journal of Engineering Geology and Environment Book Series* (6), © 2013 Sapienza Università Editrice. https://doi.org/10.4408/ijege.2013-06.b-56.

Paronuzzi, P., & Bolla, A. (2012). The prehistoric Vajont rockslide: An updated geological model. *Geomorphology, 169–170*(2012), 165–191. https://doi.org/10.1016/j.geomorph.2012.04.021.

Petronio, L., Boaga, J., & Cassiani, G. (2016). Characterization of the Vajont landslide (North-Eastern Italy) by means of reflection and surface wave seismics. *Journal of Applied Geophysics, 128,* 58–67. https://doi.org/10.1016/j.jappgeo.2016.03.012.

Pinyol, N. M., & Alonso, E. E. (2010). Thermo-hydro-mechanical and scale effects in Vaiont case. *Engineering Geology, 114*(2010), 211–227. https://doi.org/10.1016/j.enggeo.2010.04.017.

Rossi, D., & Semenza, E. (1965). *Carte geologiche del versante settentrionale del Monte Toc e zone limitrofe, prima e dopo il fenomeno di scivolamento del 9 ottobre 1963, scala 1:5000.* Istituto di Geologia: Università di Ferrara, Ferrara.

Selli, R., & Trevisan, L. (1964). Caratteri e interpretazioni della frana del Vajont. *Giornale di Geologia, Annali del Museo Geologico di Bologna, XXXII*, 7–68 **(in Italian)**.

Semenza, E., & Ghirotti, M. (2000). History of the 1963 Vajont slide: the importance of geological factors. *Bulletin of Engineering Geology and the Environment, 59,* 87–97.

Sitar, N., MacLaughlin, M. M., & Doolin, D. M. (2005). Influence of kinematics on landslide mobility and failure mode. *Journal of Geotechnical and Geoenvironmental Engineering, 131*(6), 716–728.

Superchi, L. (2012), The Vajont rockslide: new techniques and traditional methods to re-evaluate the catastrophic event. PhD Thesis, Padova University, Italy, pp 215.

Tika, Th E, & Hutchinson, J. N. (1999). Ring shear tests on soil from the Vajont landslide slip surface. *Geotechnique, 49,* 59–74.

Tinti, S., Bortolucci, E., & Vannini, C. (1997). A block-based theoretical model suited to gravitational sliding. *Natural Hazards, 16,* 1–28.

Tinti, S., Pagnoni, G., & Zaniboni, F. (2006). The landslides and tsunamis of 30th December 2002 in Stromboli analysed through numerical simulations. *Bulletin of Volcanology, 68,* 462–479.

Tinti, S., Pagnoni, G., Zaniboni, F., & Bortolucci, E. (2003). Tsunami generation in Stromboli and impact on the south-east Tyrrhenian coasts. *Natural Hazards and Earth Systems Sciences, 3,* 299–309.

Vardoulakis, I. (2002). Dynamic thermo-poro-mechanical analysis of catastrophic landslides. *Geotechnique, 52,* 157–171.

Ward, S., & Day, S. (2011). The 1963 landslide and flood at Vajont reservoir Italy. A tsunami ball simulation. *Italian Journal of Geosciences, 130,* 16–26. https://doi.org/10.3301/IJG.2010.21.

Wolter, A., Stead, D., & Clauge, J. J. (2014). A morphologic characterisation of the 1963 Vajont Slide, Italy, using long-range terrestrial photogrammetry. *Geomorphology, 206,* 147–164. https://doi.org/10.1016/j.geomorph.2013.10.006-.

Wolter, A., Stead, D., Ward, B. C., Clague, J. J., & Ghirotti, M. (2015). Engineering geomorphological characterisation of the Vajont Slide, Italy, and a new interpretation of the chronology and evolution of the landslide. *Landslides*. https://doi.org/10.1007/s10346-015-0668-0.

Zaniboni, F., Paparo, M. A., & Tinti, S. (2013). The 1963 Vajont landslide analysed through numerical modeling. *Italian Journal of Engineering Geology and Environment Book Series* (6), © 2013. Sapienza Università Editrice. https://doi.org/10.4408/ijege.2013-06.b-60.

Zaniboni, F., & Tinti, S. (2014). Numerical simulations of the 1963 Vajont landslide, Italy: Application of 1D Lagrangian modelling. *Natural Hazards, 70,* 567–592. https://doi.org/10.1007/s11069-013-0828-2.

Zhao, T., Utili, S.,& Crosta, G. B. (2016). Rockslide and impulse wave modelling in the Vajont reservoir by DEM-CFD analyses. *Rock Mechanics and Rock Engineering*. https://doi.org/10.1007/s00603-015-0731-0.

(Received April 5, 2018, revised October 9, 2018, accepted October 13, 2018, Published online October 22, 2018)